Nanoscale

Effect of AlGaN undershell on the cathodoluminescence properties of coaxial GaInN/GaN multiple-quantum-shells nanowires

Journal:	*Nanoscale*
Manuscript ID	NR-ART-08-2019-007271.R1
Article Type:	Paper
Date Submitted by the Author:	26-Sep-2019

Complete List of Authors:	Lu, Weifang; Meijo University, Department of Materials Science and Engineering Sone, Naoki; Meijo University, Department of Materials Science and Engineering Goto, Nanami; Meijo University, Department of Materials Science and Engineering Iida, Kazuyoshi; Meijo University, Department of Materials Science and Engineering Suzuki, Atsushi ; Meijo University, Department of Materials Science and Engineering Han, Dong-Pyo; Meijo University, Department of Materials Science and Engineering Iwaya, Motoaki ; Meijo University, Department of Materials Science and Engineering Tekeuchi, Tetsuya ; Meijo University, Department of Materials Science and Engineering Kamiyama, Satoshi; Meijo Daigaku, Department of Materials Science and Engineering Akasaki , Isamu; Meijo University, Department of Materials Science and Engineering; Nagoya University, Akasaki Research Center, Nagoya University

Effect of AlGaN undershell on the cathodoluminescence properties of coaxial GaInN/GaN multiple-quantum-shells nanowires

Weifang Lu[1*], Naoki Sone[1,3], Nanami Goto[1], Kazuyoshi Iida[1,4], Atsushi Suzuki[1], Dong-Pyo Han[1], Motoaki Iwaya[1], Tetsuya Tekeuchi[1], Satoshi Kamiyama[1], and Isamu Akasaki [1,2]

[1]Department of Materials Science and Engineering, Meijo University, 1-501 Shiogamaguchi, Tenpaku-ku, Nagoya, 468-8502, Japan
[2]Akasaki Research Center, Nagoya University, Furo-cho, Chikusa-ku, Nagoya 460-8601, Japan
[3] Koito Manufacturing Co., LTD., Tokyo 108-8711, Japan
[4] Toyota Gosei Co., Ltd., Aichi 452-8564, Japan
**Email: nianyulu@outlook.com, weif@meijo-u.ac.jp*

Abstract: Coaxial GaInN/GaN multiple-quantum-shells (MQSs) nanowires (NWs) were grown on an n-type GaN/sapphire template employing selective growth by metal-organic chemical vapour deposition (MOCVD). To improve the cathodoluminescence (CL) emission intensity, an AlGaN shell was grown underneath the MQS active structures. By controlling the growth temperature and duration, an impressive and up to 11-fold enhancement of CL intensity is achieved at the top area of the GaInN/GaN MQS NWs. The spatial distribution of Al composition in the AlGaN undershell was assessed as a function of position along the NW and analysed by energy-dispersive X-ray measurement and CL characterisation. By introducing an AlGaN shell underneath GaInN/GaN MQS, the diffusion of point defects from the n-core to MQS is effectively suppressed because of the lower formation energy of vacancies-complexes in AlGaN in comparison to GaN. Moreover, the spatial distribution of Al and In was attributed to the insufficient delivery of gas precursors to the bottom of the NWs and the anisotropy diffusion on the nonpolar *m*-planes. This investigation can shed light on the effect of the AlGaN undershell on improving the emission efficiency of NW-based white and micro-light-emitting diodes (LEDs).

1. Introduction

High-quality GaN and related alloys are regarded as promising materials for future lighting technologies [1-3]. In the past decade, GaN-based nanowires (NWs) were the subject of intensive research as they exhibit certain advantages in terms of improvements for material quality and light extraction efficiency [4-6]. In comparison with planar GaN thin films, the strain caused by different thermal expansion coefficients is remarkably reduced by the inherent geometry of NW structures [7]. The incorporation of In in GaInN/GaN multiple-quantum-shells (MQSs) grown on NWs can be augmented to elongate the emission wavelength and obtain phosphor-free white light emission [8, 9]. In particular, the coaxial MQS NW structure can substantially enlarge the effective active area for carrier recombination, improving the efficiency of GaInN-based light-emitting diodes (LEDs) [7, 10]. Moreover, by taking advantage of the nonpolar surface orientation (m-plane), the GaInN/GaN core-shell NWs have the potential to overcome the efficiency droop, known as a result of the quantum confined Stark effect in conventional *c*-plane LEDs [11, 12]. On the basis of these advantages, significant efforts have been made to obtain optimal structural and optical properties for efficient NW-based blue and white LEDs, as well as laser diodes (LDs) and micro-LEDs [13-17].

Despite the many advantages of GaN-based NWs, point defects are considered to detrimentally impact the performance of NW devices because of factors that provide parasitic current paths, reduce the radiative efficiency, and increase the low-frequency noise [18, 19]. Theoretical research conducted on the spatial distribution of vacancies in NW structures revealed that the formation energy of vacancies at the surface or near the edge of the *m*-planes is much lower than that in bulk GaN [20, 21]. Hence, the Ga and N vacancies preferentially form at the surface of NWs, and subsequently, multiple vacancies tend to cluster into vacancy-related complexes. Experiments showed that the major intrinsic property of nonradiative recombination centres (NRCs) in n-type GaN is divacancies comprising a Ga vacancy and an N vacancy, whereas p-type GaN mainly contains multiple vacancies-complexes [19, 22, 23]. To suppress the density of NRCs, several approaches have been implemented to trap the surface defects in conventional planar LEDs, including utilising a GaInN underlayer, an AlInN underlayer or GaInN/GaN superlattice structures [24, 25]. Impressive improvements were considered be attributed to a lower formation energy of vacancies in GaInN or AlInN in comparison to GaN as the formation energy drastically decreases with the increase in In incorporation [26]. To further improve the performance of GaInN/GaN core-shell NW-based LEDs, it is essential to suppress the diffusion of point defects from the GaN core NW into the MQS active region during growth. However, there are only few reports on employing interlayers in NWs to supress the migration of point defects into GaInN/GaN MQS [27, 28]. Typically, the AlGaN layer is used as an electron-blocking layer to improve the electron confinement within the active region in both planar and NW-based LEDs [16, 29-31]. An AlGaN film has lower surface mobility of Al because of the higher bond energy of Al–N (2.88 eV) in comparison to Ga–N (2.2 eV) [32]. Moreover, the formation energy of vacancies is rather low, and strongly decreases with increasing Al incorporation, which makes the AlGaN layer definitely suitable for trapping defects [22, 33, 34].

In this study, we investigate the effect of the AlGaN undershell on the morphology and cathodoluminescence (CL) properties of GaInN/GaN MQS NWs. In an attempt to suppress the mitigation of vacancies, the growth temperature and thickness of the AlGaN layer grown on n-type GaN NWs was systematically adjusted, followed by the growth of five pairs of GaInN/GaN MQSs. The epitaxial growth, morphology and CL enhancement of coaxial GaInN/GaN NWs were systematically discussed by analysing energy-dispersive X-ray (EDX) mapping of the element distribution and spatially-resolved CL spectra. The analysis revealed that the Al composition and the thickness of AlGaN are crucial factors for trapping of point defects. The spatial distribution of CL enhancement in NWs was interpreted as a consequence of the Al incorporation in the AlGaN undershell as well as In gradient distribution along the nonpolar *m*-planes. The growth mode of AlGaN undershells on *m*-planes under different growth conditions has been proposed.

2. Experimental details for NW growth by MOCVD

To prepare the dielectric mask array for selective-area growth, a 30-nm thick SiO_2 layer was deposited on the commercial GaN/sapphire template (NANOWIN Co., China) by using a radiofrequency magnetron sputtering system (CFS-4EP, Shibaura Mechatronics Co., Japan). Then, spin-coating with a polymer resist (CELV SOL003, DAICEL Co., Japan) and nanoimprint lithography (TEX-01, KYODO INTERNATIONAL INC., Japan) were performed to form an aperture array pattern. Subsequently, the SiO_2 layer was etched by inductively coupled plasma (ICP) etching (CE-300I, ULVAC Co., USA), forming an aperture array with a diameter and a pitch distance of 320 nm and 1200 nm, respectively. Afterwards, the residual polymer resist on the surface was completely cleaned to remove any impurities using a standard etchant consisting of a mixed solution of H_2SO_4 and H_2O_2 in a 1: 1 ratio. Lastly, the substrate was dried in an N_2 flow and transferred into the reactor to proceed with epitaxial growth. The aperture structures were characterised by three-dimensional (3D) visualisation measurements using a four-segment backscattered electron detector in a scanning electron microscope (SEM-SU5000, Hitachi Co., Japan), as shown in Figure 1(a). The depth of the aperture array is larger than 30 nm, which confirmed that the GaN substrate under the aperture array is entirely exposed and slightly over-etched.

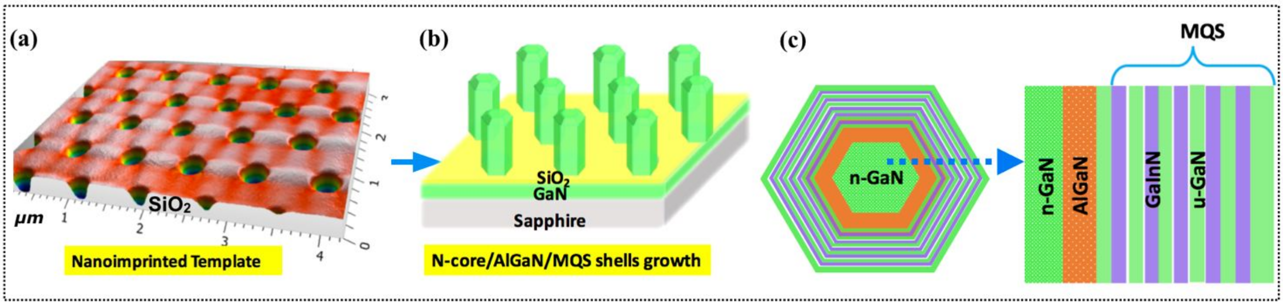

Figure 1 (a) 3D topography of the aperture array on the nanoimprinted template, measured using a four-segment backscattered electron detector. (b) Schematic illustration of the grown NWs consisting of n-core, AlGaN and MQS shells. (c) Detailed planar cross-section of the NW, including the n-GaN core, AlGaN undershell, and five pairs of GaInN/GaN quantum shell structures.

After preparing a SiO_2 mask layer on the GaN/Sapphire template, a horizontal MOCVD system equipped with a 2-in susceptor (SR 2000, TAIYO NIPPON SANSO Co., Japan) was employed to carry out the growth process for core-shell NWs. The coaxially aligned n-GaN core/AlGaN undershell/GaInN/GaN MQS NWs are shown in the schematic diagrams in Figure 1(b) and (c). First, n-type GaN core NWs were grown on the template by using continuous-flow mode in MOCVD. Trimethylgallium (TMG) and ammonia (NH_3) were used as the precursors for the Ga and N source, respectively. The typical growth temperature for core NWs was maintained at 1135 °C. The dopant precursor of SiH_4 was injected at a rate of 1.25 sccm (2.79×10^{-3} μmol/min) sccm with the H_2 carrier gas. The growth pressure was maintained at 90 kPa. The growth duration was 1.5 min, where the TMG and NH_3 flow rates were fixed at 50 sccm and 100 sccm (V/III = 20). Core NWs with 380-nm in diameter and 1.3 μm in height were obtained. A conformal AlGaN undershell was coaxially grown on the core NWs at 740 °C for 10.6 min. A triethylgallium (TEG) flow rate of 250 sccm, an NH_3 flow rate of 6000 sccm and a trimethylaluminium (TMA) flow rate of 4 sccm were used to provide the precursors with N_2 as the carrier gas at a pressure of 90 kPa. Afterwards, five pairs of MQS composed of an approximately 5-nm thick barrier and a 3.5-nm thick well were grown sequentially at 740 °C. In this process, the TEG and NH_3 flow rates were kept at 30 sccm and 3000 sccm, respectively.

Table 1. MOCVD Growth Parameters for NW Samples

Samples I: n-core/AlGaN	Samples II: n-core/AlGaN/MQS	Temperature of AlGaN(10.6 min)	Samples III: n-core/AlGaN	Samples IV: n-core/AlGaN/MQS	Growth time of AlGaN (740 °C)
a_1	a_2	740 °C	a_3	a_4	30 s
b_1	b_2	840 °C	b_3	b_4	10.6 min
c_1	c_2	940 °C	c_3	c_4	21.2 min
d_1	-	1140 °C	d_3	d_4	31.8 min

To investigate the effect of growth temperature and thickness of the AlGaN undershell on the morphology and CL properties, four different batches of NW samples were prepared, as shown in Table 1. The first batch of samples (a_1–d_1) was composed of n-core NWs structures and the AlGaN undershell grown at different temperatures from 740 °C to 1140 °C. The second batch of samples (a_2–d_2) involved the additional growth of MQS under the same condition. To investigate the effect of AlGaN thickness, the growth time of AlGaN for batches a_3–d_3 and a_4–d_4 was varied from 30 s to 31.8 min, respectively. For comparison, a reference sample (marked as R_0) without the AlGaN shell underneath was grown under the same condition of the core and MQS (740 °C). The growth conditions of the well and barrier shells were the same for all NW samples covered with GaInN/GaN MQS. The surface morphology and Al composition depending on the growth temperature, were characterised by SEM and CL measurements. To evaluate the effect of the AlGaN undershell on the luminescent properties of the coaxial GaInN/GaN MQS, spatially resolved panchromatic CL mapping and spectra were analysed.

3. Results and discussions

3.1 Morphology of AlGaN shell and Al content characterisation

The surface morphology of the NW samples a_1–d_1 was characterised by using a SEM system (SU70, Hitachi High-Technologies Co., Japan) operated at 3 kV. The NWs are grown perpendicular to the *c*-plane of the substrate and exhibit hexagonal structures with six smooth nonpolar sidewalls, as shown in Figure 2. As the growth temperature is increased, the crystal growth on the SiO_2 mask layer is suppressed and the *c*-plane becomes smooth. In AlGaN growth, Al adatoms were reported to have a much larger sticking coefficient and less surface mobility than Ga adatoms [35]. In addition, Ga adatoms can diffuse a much longer distance of ~0.7–5 μm than Al adatoms due to the weak Ga-N bonds [30, 36]. Hence, at low temperature, the crystal growth on the mask layer is attributed to the short diffusion length of the Al–Ga adatom groups on the *c*-plane and mask layer. The lateral growth rate (diameter) increased as the temperature elevated, and the growth rate on the semipolar plane of the bottom area was relatively lower, as shown in Figure 2(d_{ii}). The decomposition rate was significantly enhanced, which decreased the diffusion rate from the mask layer to the bottom of the NWs. Simultaneously, the growth on the *c*-plane was suppressed owing to the higher decomposition rate and larger diffusion length at higher temperatures.

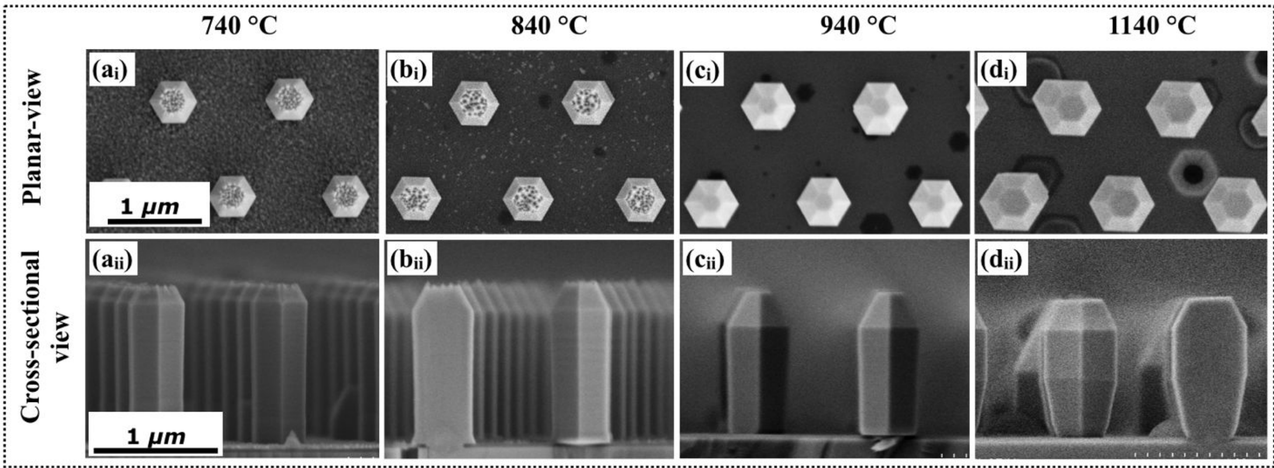

Figure 2 Planar and cross-sectional view SEM images of the NW samples a_1, b_1, c_1, and d_1, respectively, where the AlGaN undershells were grown for 10.6 min at different temperatures.

Compositional analysis was performed by EDX in the SEM (SU5000, Hitachi Co., Japan) with an accelerating voltage of 10 kV. The EDX mappings of Ga, N, Al and Si are shown in Figure 3(a). Higher Al densities were detected at the top areas of the NWs than that at the bottom parts, where the Ga and N elements exhibit a complimentary distribution (see Figures 3(a_1)–(a_4)). The growth of the AlGaN crystal on the SiO_2 mask layer is likewise confirmed by the spatial distribution of all elements. To quantify the Al content, CL measurements were taken at an accelerating voltage of 7 kV with a beam current of 35 μA in the SEM system (SU70, Hitachi Co., Japan). Figure 3(b) shows the CL emission spectra at the top and bottom areas of *m*-plane in sample a_1. The bandgap emission spectra (~ 360 nm) distinguish as two separate peaks, which refer to the emissions from the AlGaN shell and GaN core, respectively. The yellowish peak at 535 nm is typically attributed to deep level defects in the GaN core NWs [18]. The bandgap emission peaks of samples a_1, b_1, c_1 and d_1 are normalised and calibrated according to the n-core GaN emission peak at 369 nm. Subsequently, the CL spectra were fitted by two Gaussian functions to separate the two emission peaks of AlGaN and GaN, respectively. Theoretically, the bandgap of AlGaN can be expressed as follows [37]: $Eg\ (\text{AlGaN}) = x \cdot Eg\ (\text{AlN}) + (1–x) \cdot Eg\ (\text{GaN}) + b \cdot x \cdot (1–x)$, where Eg (AlGaN), Eg (AlN) (6.2 eV) and Eg (GaN) (3.4 eV) are the bandgaps of AlGaN, AlN, and GaN, respectively. The value of bowing parameter b = 1 eV was used to estimate the Al mole fraction in AlGaN undershells grown at different temperatures [38]. Figure 3(c) shows a plot of the Al incorporation in the AlGaN undershell at the top and bottom positions of NWs as a function of growth temperature. In comparison to the top area, the emission peak of NWs at bottom area exhibits redshift due to lower Al incorporation. The Al content of the top area is decreased from 5.9% to 0.43% as the growth temperature increases from 740 °C to 1140 °C. Because of the larger sticking coefficient, less mobility, and shorter diffusion length of Al in comparison to Ga [32, 35], it is deduced that Al adatoms favour incorporation at the top areas (especially at lower temperatures). As the growth temperature increases, both the decomposition rate and diffusion length increase, which significantly suppresses the growth on the mask layer. This phenomenon is in accordance with the SEM morphology shown in Figure 2. Moreover, the diameter of sample d_1 is larger than that of other samples, which suggests that the growth rate might also affect the decrease in Al content [39]. The mechanism of such growth phenomena will be further discussed in the following section.

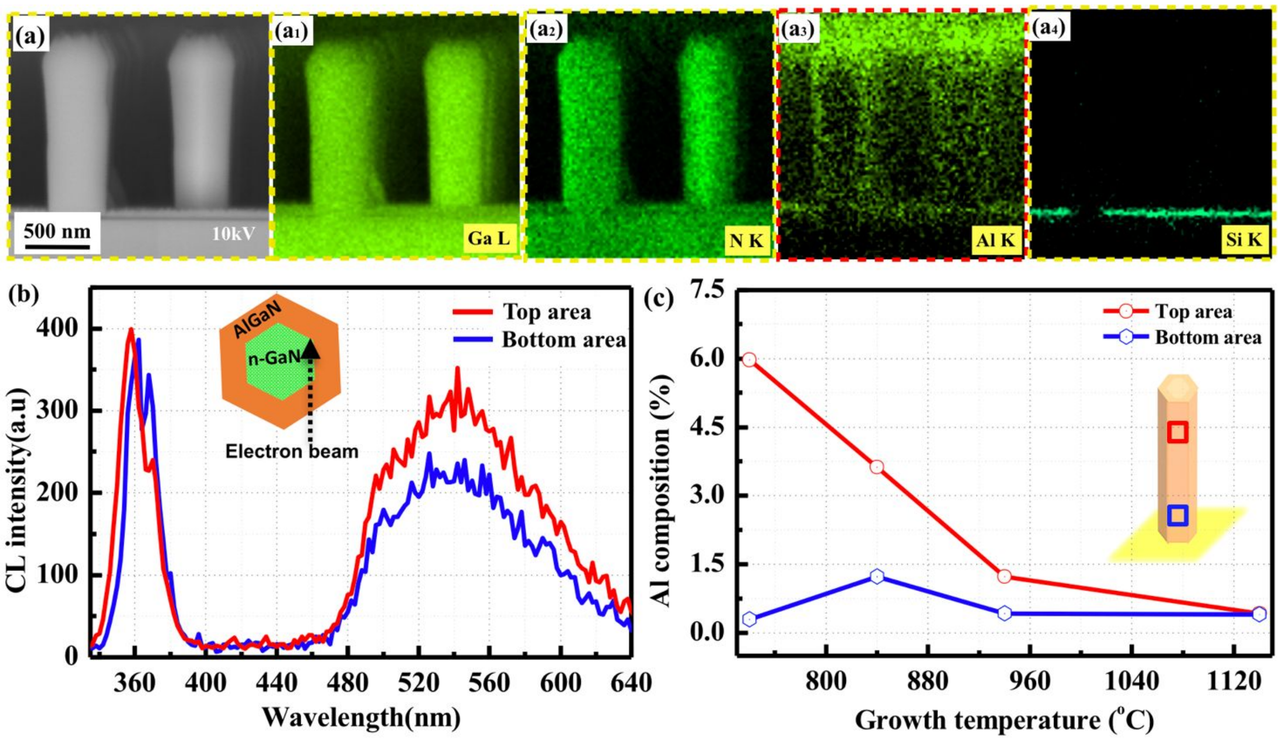

Figure 3 (a) EDX mapping of Ga, N, Al and Si on the NW samples grown at 740 °C. (b) CL spectra measured at the top and bottom areas of NWs in sample a_1. (c) Al composition percentage on the top (red) and bottom (blue) areas of the NW as a function of growth temperature of AlGaN shells.

3.2 CL enhancement in NWs with AlGaN undershell

The optical properties of as-grown coaxial GaInN/GaN NW arrays were probed by CL measurements in the SEM system. The probe current was set to 35 μA with an accelerating voltage of 7 kV. The CL signal was collected by a parabolic mirror and analysed with a filter/detector system (Gatan MonoCL4) equipped with a charge-coupled device cooled with liquid nitrogen. The measurements in this study were carried out at room temperature. The uniformity of the samples was qualitatively checked in terms of panchromatic CL mapping at different positions of the samples. For quantitative analysis, the CL spectra from the top, middle and bottom positions of one NW and the corresponding spatially resolved panchromatic CL mapping of the sample a_2 are depicted in Figure 4. The existence of two distinct peaks (located at 440 nm and 500 nm) in the top area of the NW indicates the presence of the regions with different In concentrations. The blue peak can be ascribed to the emission of the MQS on the *m*-planes, whereas the green peak arises from the In-rich region at the junction between the *m*-planes. From Figures 4(a) and 4(c), it is confirmed that the CL emission intensity has a significant ~11-fold enhancement at the top area of the NW in sample a_2 compared with the reference sample R_0. However, the CL enhancement at the bottom area is weeny in comparison to the top part of the NW. The CL studies provide evidence of an In gradient in these NW structures because the emission peak exhibits a significant blueshift from the top area to the bottom areas. Moreover, the CL intensity of GaN-related band edge emission peaks increased in sample a_2, due to the reduced NRCS density in MQS region.

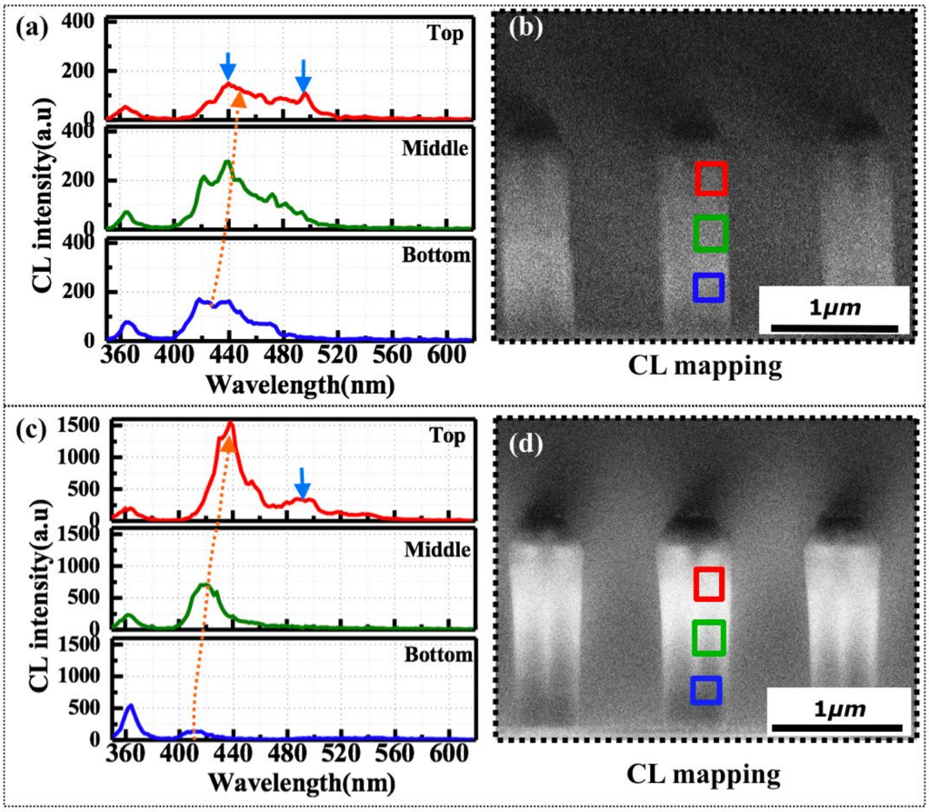

Figure 4 CL emission spectra of the top, middle and bottom positions on the (a) reference NW sample R_0 and (c) sample a_2. The panchromatic CL mapping in (b) and (d) shows the corresponding measurement positions for CL spectra.

Assuming that the increase of the CL emission intensity is related to the AlGaN undershell, it is essential to further investigate the effect of Al content in the AlGaN undershell on the MQS emission properties of NWs. The growth temperature has been shown to affect the Al incorporation rate on *m*-planes in Section 3.1. Hence, MQS NW samples a_2, b_2, and c_2 with AlGaN undershells grown at different temperatures were prepared. Figures 5(a) and (b) show the evolution of CL emission wavelength and intensity in NW samples R_0, a_2, b_2, and c_2 as a function of measurement position from the top to the bottom area. In Figure 5(a), a blueshift can be observed from the top to the bottom in all samples, mainly owning to the insufficient precursor diffusion to the bottom region during growth. Moreover, the In incorporation (blueshift) is affected by utilising an AlGaN undershell grown at different temperatures, which might be related to the increased diameter of the NWs. Thus, the thickness of the MQS should be taken into account for a comprehensive analysis combining structural and optical properties, as plotted in Figure 5(c). The thickness of MQS in samples R_0 and b_2 was further verified by scanning transmission electron microscopy (STEM). The measurements were carried out using a Hitachi HD2700 STEM system (Hitachi High Technologies Cor. Japan) with an acceleration voltage of 200 kV. Figures 5(d) and 5(e) show the MQS thickness measured at the top, middle, and bottom positions. Thus, it can be confirmed that the thickness of MQS decreases in NW samples as a function of the position from the top to bottom area. Comparison of the curves in Figures 5(a) and (c) shows that the tendency of emission wavelengths for samples R_0, a_2, b_2, and c_2 is similar to that of MQS thickness at different positions of NWs. Therefore, the blueshift of emission peak at the same position for samples with or without the AlGaN shell is mainly caused by the variation of diameter at different positions. This indicates that the In incorporation is proportional to the MQS thickness and affected by the AlGaN shells (diameter) grown at different temperatures.

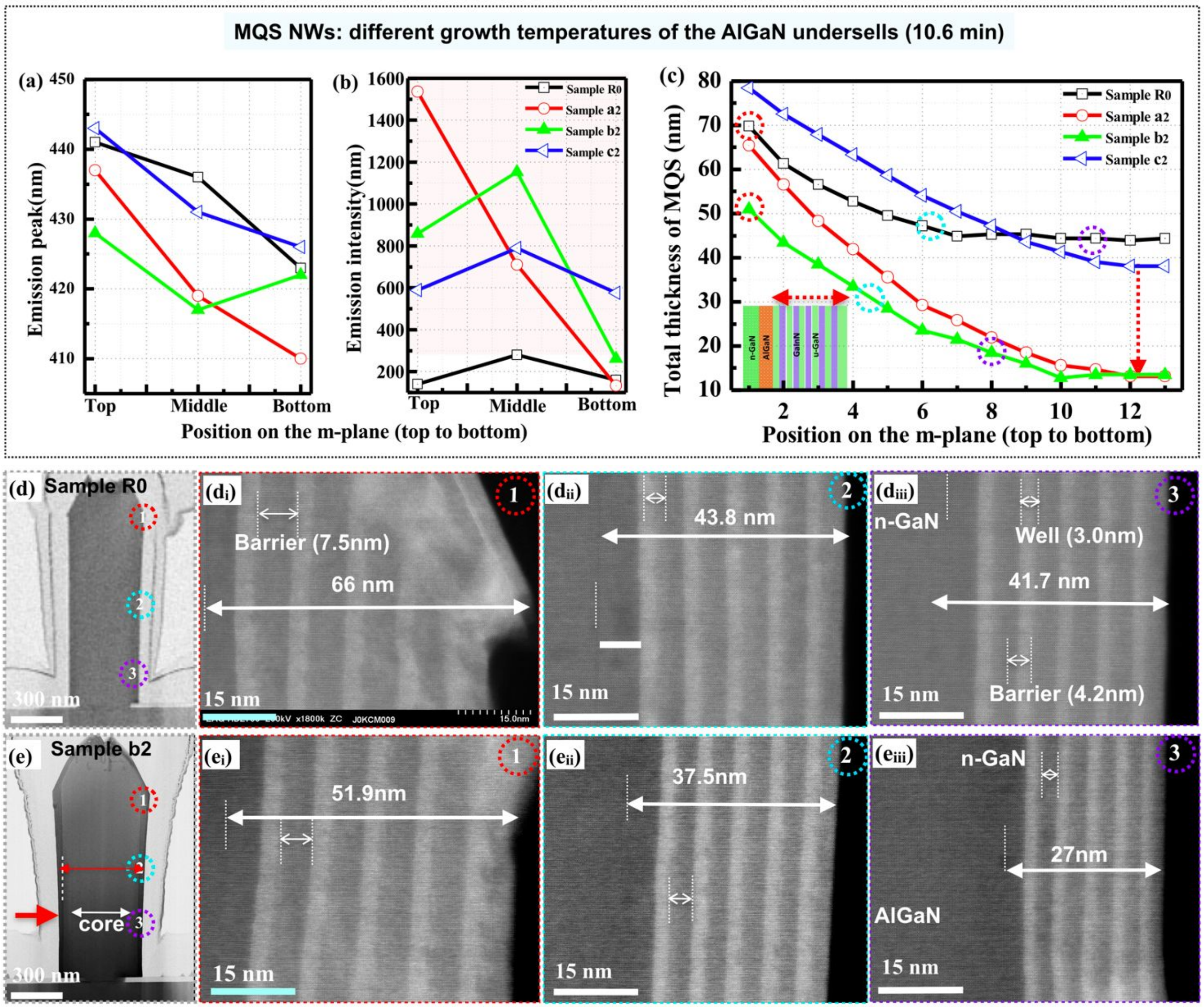

Figure 5 (a) CL emission peaks and (b) CL intensities for reference sample R_0 and samples a_2, b_2, and c_2 as a function of the position on the *m*-plane (from top to bottom). (c) Relationship between total thicknesses of MQS and positions as a function from the top to bottom areas of NW samples a_2, b_2, c_2 and d_2. (d) and (e) show the STEM images of samples R_0 and b_2, where the thickness of MQS (including the first barrier) is marked.

Regarding the CL enhancement in Figure 5(b), it can be deduced that the CL enhancement on NWs with the AlGaN undershell is attributed to the spatial distribution of Al incorporation, as well as the growth temperature of AlGaN shells. The smaller enhancement at the bottom area is related to lower Al incorporation at the bottom area of the NWs. Moreover, because AlGaN crystal was grown on the SiO_2 mask layer (rough surface) for samples a_2 and b_2, fewer precursors can diffuse towards the bottom area of the NWs, resulting in an extremely thin layer of MQS. The comparison between the CL enhancement and the Al composition in Figure 2 provides a complete picture of the emission in NW samples with an AlGaN undershell grown at different temperatures. Thus, one can speculate that the diffusion of precursors towards the bottom part is the dominant growth mechanism for MQS growth in these areas.

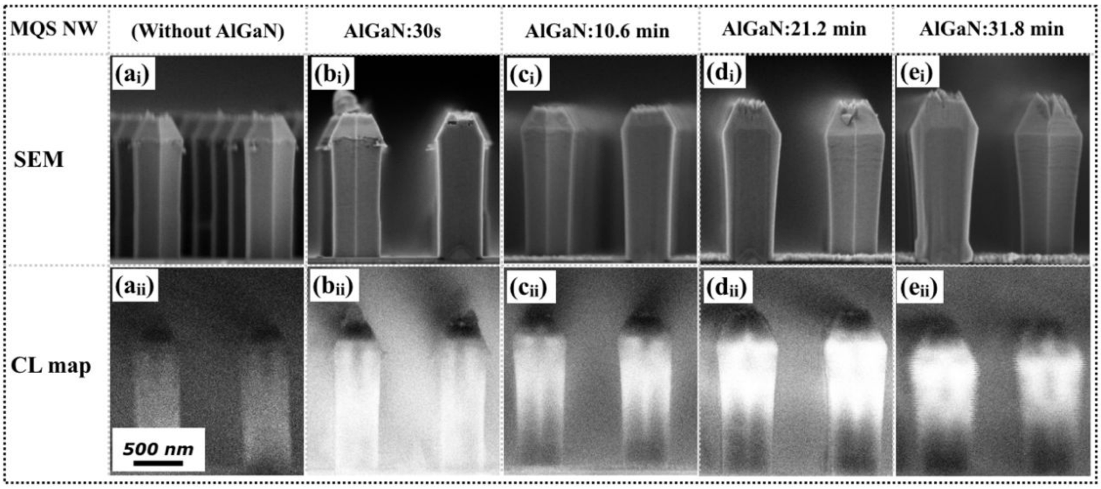

Figure 6 Cross-sectional view SEM images of the NW samples (a_i) R_0, (b_i) a_4, (c_i) b_4, (d_i) c_4, and (e_i) d_4. The corresponding panchromatic CL mappings are shown underneath (a_{ii})–(e_{ii}).

The optimal growth temperature of the AlGaN undershell is 740 °C, inducing a CL enhancement that is as high as 11-fold at the top part of the MQS NWs. Nevertheless, the crystal growth on the mask layer might deteriorate the spatial distribution of Al incorporation and followed by MQS growth. In addition to the growth temperature of AlGaN, the layer's thickness was investigated to further evaluate the effect of AlGaN undershell. Samples a_3, b_3, c_3 and d_3 grown with different durations of AlGaN undershells were prepared to the end, and the diameter was found to be linearly increasing with the growth time. The estimated growth rates were around 3.7 nm/min and 1.4 nm/min at the top and bottom parts of the NWs, respectively. Therefore, the thickness of AlGaN undershell grown for 30 s was estimated to be ~2 nm. Subsequently, samples a_4, b_4, c_4 and d_4 covered with the AlGaN shells with different growth times were subjected to MQS growth. The cross-sectional SEM images of the samples R_0, a_4, b_4, c_4, and d_4 are shown in Figures 6(a_i), (b_i), (c_i), (d_i) and (e_i), respectively. Few In-rich droplets can be observed in samples R_0 and a_4, and this phenomenon can be eliminated with thick AlGaN undershells. However, the thickness of the crystal on the SiO_2 mask layer increased, and the spatial distributions of CL emissions became more obvious. The corresponding CL mappings in Figures 6(a_{ii})–(e_{ii}) reveal that the emission intensity increased with using different thicknesses of AlGaN undershells, especially at the top area of the NWs. The spatial distribution of the CL emission in sample a_4 is more uniform than that of the other samples.

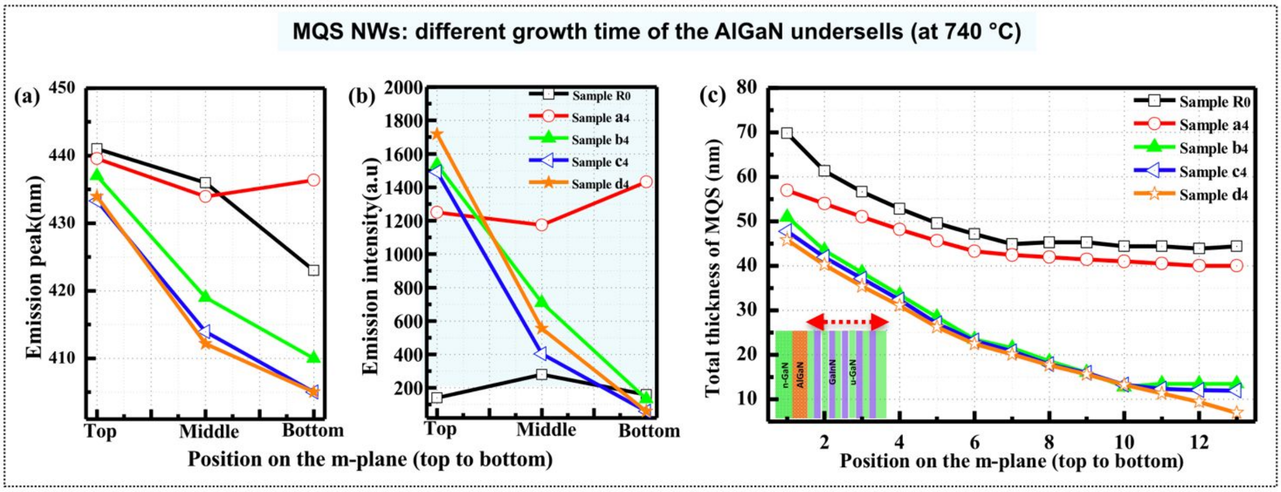

Figure 7 (a) CL peak wavelength and (b) intensities in samples R_0, a_4, b_4, c_4 and d_4 as a function of position on the *m*-plane (from top to bottom area). (c) Relationship between the total thickness of MQS shells and the position on the *m*-plane of NW samples R_0, a_4, b_4, c_4 and d_4.

The evolution of CL emission wavelength and intensity in NW samples R_0, a_4, b_4, c_4 and d_4 as a function of position from the top to the bottom area is shown in Figures 7(a) and (b). The emission peak reveals an obvious blueshift from the top to the bottom area, which is ascribed to the gradient of In incorporation in the NWs. The total thickness of MQS was calculated according to the diameter of samples a_3–d_3, R_0, and a_4–d_4, as plotted in Figure 7(c). A contrastive analysis was carried out by horizontal comparison (comparing the variation in the same NW from the top to bottom) and longitudinal comparison (same position in different NW samples). The distribution of emission intensities in Figure 7(b) shows that the CL intensity at the top part of the NW increases with the thickness of the AlGaN undershell. Although the CL intensity decreases as well as the thickness of MQS, the thickness of AlGaN concurrently decreases from the top to bottom of NWs (Samples b_4–d_4). This indicates that the enhancement of the emission intensity is mainly related to the incorporation of point defects in the AlGaN undershells depending on the thickness. This phenomenon further demonstrates the essential role of the AlGaN undershells in suppressing the diffusion of vacancies into MQS structures. Moreover, the stable emission peak and uniform intensity in sample a_4 reveal that the ultra-thin AlGaN undershell (~2 nm) is advantageous for trapping point defects, as well as maintaining a favourable geometry (the thickness of MQS). The In composition in the InGaN/GaN MQS grown under the same conditions exhibits slight differences with different thicknesses of the AlGaN undershells. Therefore, the enhanced CL emission intensity at the bottom areas of the NWs in sample a_4 is ascribed to the thicker MQS structure and effect of AlGaN undershell. The phenomenon at the bottom part of NWs is similar to that in Figure 5(b), which demonstrates once more the influence of the lower Al incorporation and low growth rate of MQS shells. Hence, the thin AlGaN undershell is favourable for both the CL enhancement and spatial uniformity in coaxial NW structures.

3.3 Discussion

A comprehensive investigation of structural and optical properties has been performed in the previous sections. The diffusion processes of vacancies on the *m*-planes of NWs with and without the AlGaN undershell are schematically illustrated in Figures 8(a) and (b), respectively. Because the GaN core NWs were grown under Ga-rich conditions (V/III = 20) and at high temperature, numerous point defects were present at the surface, which diffused and be incorporated into the GaInN /GaN MQS, as depicted in Figure 8(a). The intrinsic purpose of the AlGaN undershell is to trap these vacancies, since it has a lower formation energy and creates vacancy–complexes easier than GaN. Consequently, only few vacancies can diffuse into GaInN /GaN MQS, as shown in Figure 8(b). Thus, an enhancement of the CL intensity is expected in NW samples with the AlGaN undershell. The formation energy of vacancies in AlGaN decreases with increasing Al content [33, 40] such that the AlGaN undershell with higher Al content can trap more NRCs [34]. Thus, the significant enhancement of CL intensity is attributed to the efficient trapping of point defects in the AlGaN undershell, decreasing the nonradiative recombination rate in the MQS active region [25, 26]. The dependence of CL enhancement on the Al content also implies that more point defects can be trapped because of the lower formation energy of vacancies in AlGaN with higher Al composition [33, 41]. The ultra-thin AlGaN undershell grown at low temperature can provide both high Al content and favourable spatial-uniform NW structures. However, the growth results of AlGaN on the *m*-planes are quite different in the case of *c*-plane films [42], i.e., the Al content increases with increasing temperature.

A schematic illustration of the growth of AlGaN on *m*-planes is depicted in Figure 8(c). The growth of the AlGaN undershell on core NWs is mainly determined by three factors: (i) Ga/Al adatoms impinging on the top area will incorporate directly into the crystal growth (most dominant factor), (ii) few Ga/Al atoms arriving at sidewalls will diffuse on the *m*-planes and (iii) Ga/Al atoms arriving to the SiO_2 mask layer will diffuse to the bottom area of NWs (lateral sidewalls) and incorporate into the crystal. The competition among these three factors at different growth temperatures induces different morphologies and levels of Al incorporation in NWs. Theoretically, the diffusion of Al adatoms in the *a*-axis direction has a much lower barrier (0.11 eV) than that in the *c*-axis direction (2.79 eV) [43], and the diffusion barriers for Ga are 0.21 eV (*a*-axis) and 0.93 eV (*c*-axis) [44], respectively. Thus, the spatial distribution of Al composition can be attributed to the configuration of a horizontal flow in MOCVD reactor and a shorter diffusion length of Al adatoms compared with Ga adatoms [45]. At the bottom of the NW structures, additional Ga as well as Al species are supplied by the lateral diffusion from the mask area as shown in Figure 8(c). However, at low temperatures of 740 °C, the diffusion length of the Ga–Al adatom groups decreased, resulting in a higher Al content at the top area and crystal growth on the SiO_2 mask layer. Moreover, the blueshift from the top to the bottom area of NWs can be interpreted as the gradient incorporation of In due to insufficient In diffusion to the bottom area. The blueshift of the CL emission peak with an elevated growth temperature of AlGaN is ascribed to the slightly increased diameter of the NWs. Because the precursors and growth conditions for MQSs remained constant (total volume), the grown thickness slightly decreased with a lower density of In incorporation. This phenomenon is in accordance with that in the samples grown at different thicknesses of the AlGaN shell at 740 °C. Therefore, the uniformity of AlGaN and MQS in sample a_4 is better than the other NW samples with thicker AlGaN undershell. At higher growth temperature (> 840 °C), the uniformity of Al and In incorporation along the sidewalls of NWs can be improved by increasing the pitch size between aperture holes, since more adatoms arriving at SiO_2 mask layer are able to diffuse to the bottom area of NWs.

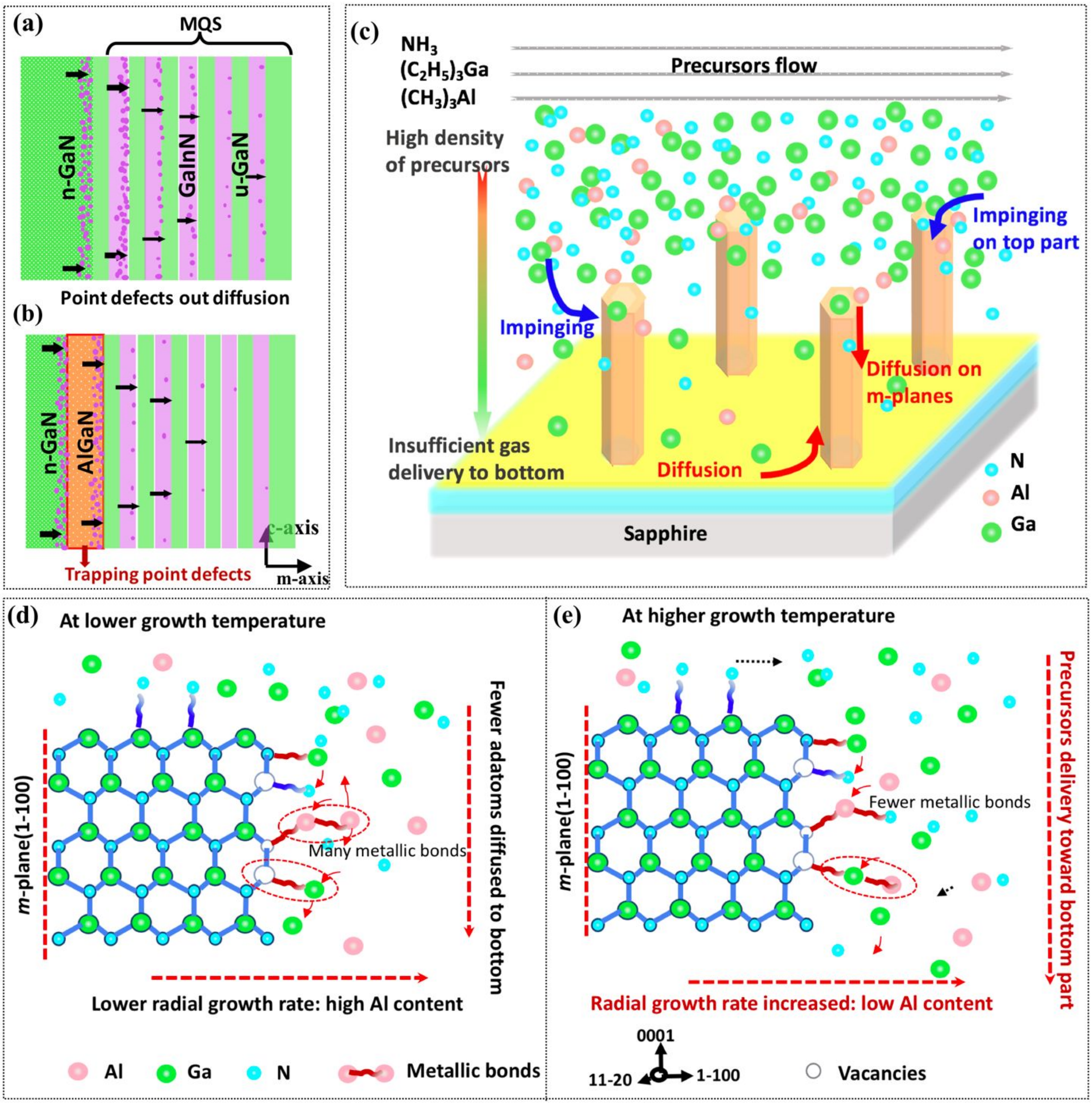

Figure 8 Schematic illustrations showing (a) the point defect diffusion process during the growth of GaInN/GaN MQS on *m*-planes of NWs and (b) effect of the AlGaN undershell in trapping point defects. (c) Illustration of the growth process of the AlGaN shell on n-GaN core NWs: horizontally supplied precursors can thermally diffuse towards the top part of the NWs and chemically absorbed/impinged on the surface. The growth model of AlGaN on the *c*- and *m*-planes at low temperature (d) and higher temperature (e), referring to the theoretical calculation reported by Vibhu Jindal *et.al* and Liverios Lymperakis *et al.* [43, 44].

To provide a deep insight into the variation of Al content, further discussion is necessary regarding the diffusion properties of precursors on *m*-planes. Considering the Al incorporation, both Ga and Al atoms are expected to diffuse anisotropically on *m*-planes. According to theoretical calculations obtained from the literature, the diffusion barrier constricting the movement of Ga or Al adatoms on *m*-planes along the *c*-axis [0001] is much larger than that along the *a*-axis [43, 44]. Al adatoms have a favourable attachment to *m*-planes of the core-shell NWs owing to the stronger bonding energy in Al–N than that in Ga–N bond [46]. Impinging of Ga or Al adatoms on the *c*-plane can create a strong Ga–N or Al–N bond, because the exposed dangling bonds are dominated by N atoms. Nevertheless, the growth mechanism on the *m*-plane is quite different, as illustrated in Figures 8(d) and (e). The *m*-plane surface consists two species of Ga and N atoms, which may form either strong Ga–N/Al–N bonds or weaker metallic bonds and easily diffuse along the *a*-axis direction by breaking the metallic bonds [44]. At the low growth temperatures and a high V/III ratio of 5415 (N-rich), all metallic impinged atoms are expected to be incorporated into growth of AlGaN undershell. In that case, few precursors are delivered to the bottom area, and Al incorporation is favourable on the *m*-plane, resulting in a high Al composition. At a higher growth temperature, the diffusion of Al/Ga adatoms in the *a*-axis direction is facilitated, and few metallic bonds can be formed, enhancing the radial growth rate along the *m*-axis. In addition, more precursors can be delivered to the bottom part, resulting in a lower Al composition in the top part of the NWs. On the basic of the morphology of samples a_1, b_1, c_1, and d_1, the increase in the surface mobility of Al is particularly important for improving the uniformity and reducing the growth on SiO_2. The uniform Al or In incorporation on NWs is expected to be achievable by the pulsed-growth technique or using vertical flow MOCVD reactors.

4 Conclusion:

We demonstrated a significant enhancement of the CL emission intensity in MQS NWs in the presence of an AlGaN undershell. Coaxial GaInN/GaN NW arrays with the AlGaN undershell were grown on the aperture array pattern in the substrates using continuous-flow mode in MOCVD with a horizontal supply configuration. The relationship between growth temperature and Al incorporation was characterised and discussed by the EDX mapping and CL measurements. The decreased incorporation of Al species with increasing growth temperature of the AlGaN shell was interpreted by the anisotropic diffusion properties of Ga and Al atoms on *m*-planes. However, the increase in CL emission intensity is much higher at lower growth temperature of AlGaN undershells because of a higher Al composition. Subsequently, the coaxial GaInN/GaN NWs with different thicknesses of AlGaN undershells were investigated. The results showed that the optimal thickness of the AlGaN undershell is around ~2–5 nm as it provided significant enhancement and a quite uniform spatial distribution of CL emission across the NW. The enhanced CL emission in all samples with the AlGaN undershell reveals that the AlGaN indeed plays an important role at trapping point defects because of the lower formation energy of vacancy-complexes than in GaN. Therefore, the diffusion of point defects from the GaN core NW can be effectively suppressed to prevent their incorporation into InGaN/GaN MQSs. The spatial distribution of Al and In from the top to bottom areas of NWs is ascribed to the gradient incorporation of Al/In due to insufficient precursor diffusion to the bottom area and the low diffusion length along the *c*-axis. The feasibility of trapping point defects using an ultra-thin AlGaN undershell on *m*-plane coaxial NWs can be employed for the realisation of highly efficient white and micro-LEDs.

Author contributions

W.L. grew the NW samples, analyzed the results and wrote the manuscript. N.S., N.G. and K.I. assisted with the MOCVD growth and measured the EDX mappings. The CL measurements were performed by N.G. A.S provided the template substrate by using nanoimprint photolithography. D.H, N.S, T.T and S.K. joined in the discussion and revised the manuscript. S.K., T.T, M.I and I.A. contributed to the data analysis and supervised the project.

Acknowledgement

This work was financial supported by MEXT “Program for research and development of next-generation semiconductor to realize energy-saving society”, MEXT “Private University Research Branding Project”, JSPS KAKENHI for Scientific Research A [No.15H02019], JSPS KAKENHI for Scientific Research A [No.17H01055], JSPS KAKENHI for Innovative Areas [No.16H06416], and Japan Science and Technology CREST [No.16815710].

References:

[1] I. Akasaki, H. Amano, Breakthroughs in improving crystal quality of GaN and invention of the p–n junction blue-light-emitting diode, Japanese journal of applied physics 45 (2006) 9001.
[2] I. Akasaki, Nobel Lecture: Fascinated journeys into blue light, Reviews of Modern Physics 87 (2015) 1119.
[3] S.F. Chichibu, A. Uedono, T. Onuma, B.A. Haskell, A. Chakraborty, T. Koyama, P.T. Fini, S. Keller, S.P. Denbaars, J.S. Speck, U.K. Mishra, S. Nakamura, S. Yamaguchi, S. Kamiyama, H. Amano, I. Akasaki, J. Han, T. Sota, Origin of defect-insensitive emission probability in In-containing (Al,In,Ga)N alloy semiconductors, Nat Mater 5 (2006) 810-816.
[4] P.-M. Coulon, B. Alloing, V. Brändli, P. Vennéguès, M. Leroux, J. Zúñiga-Pérez, Dislocation filtering and polarity in the selective area growth of GaN nanowires by continuous-flow metal organic vapor phase epitaxy, Applied Physics Express 9 (2016) 015502.
[5] Y. Kurisaki, S. Kamiyama, M. Iwaya, T. Takeuchi, I. Akasaki, Theoretical investigation of nitride nanowire-based quantum-shell lasers, physica status solidi (a) 214 (2017) 1600867.
[6] M. Terazawa, M. Ohya, K. Iida, N. Sone, A. Suzuki, K. Nokimura, M. Takebayashi, N. Goto, H. Murakami, S. Kamiyama, Hybrid simulation of light extraction efficiency in multi-quantum-shell (MQS) NW (nanowire) LED with a current diffusion layer, Japanese Journal of Applied Physics 58 (2019) SCCC17.
[7] S. Li, A. Waag, GaN based nanorods for solid state lighting, Journal of Applied Physics 111 (2012) 071101.
[8] C.H. Liao, W.M. Chang, H.S. Chen, C.Y. Chen, Y.F. Yao, H.T. Chen, C.Y. Su, S.Y. Ting, Y.W. Kiang, C.C. Yang, Geometry and composition comparisons between c-plane disc-like and m-plane core-shell InGaN/GaN quantum wells in a nitride nanorod, Opt Express 20 (2012) 15859-15871.
[9] T.W. Yeh, Y.T. Lin, L.S. Stewart, P.D. Dapkus, R. Sarkissian, J.D. O'Brien, B. Ahn, S.R. Nutt, InGaN/GaN multiple quantum wells grown on nonpolar facets of vertical GaN nanorod arrays, Nano Lett 12 (2012) 3257-3262.
[10] A. Waag, X. Wang, S. Fündling, J. Ledig, M. Erenburg, R. Neumann, M. Al Suleiman, S. Merzsch, J. Wei, S. Li, H.H. Wehmann, W. Bergbauer, M. Straßburg, A. Trampert, U. Jahn, H. Riechert, The nanorod approach: GaN NanoLEDs for solid state lighting, physica status solidi (c) 8 (2011) 2296-2301.
[11] A.-J. Tzou, D.-H. Hsieh, K.-B. Hong, D.-W. Lin, J.-K. Huang, T.-P. Chen, T.-S. Kao, Y.-F. Chen, T.-C. Lu, C.-H. Chen, High-efficiency InGaN/GaN core–shell nanorod light-emitting diodes with low-peak blueshift and efficiency droop, IEEE Transactions on Nanotechnology 16 (2017) 355-358.
[12] T. Takeuchi, S. Sota, M. Katsuragawa, M. Komori, H. Takeuchi, H. Amano, I. Akasaki, Quantum-confined Stark effect due to piezoelectric fields in GaInN strained quantum wells, Japanese Journal of Applied Physics 36 (1997) L382.
[13] T.R. Kuykendall, A.M. Schwartzberg, S. Aloni, Gallium Nitride Nanowires and Heterostructures: Toward Color-Tunable and White-Light Sources, Adv Mater 27 (2015) 5805-5812.
[14] Y.J. Hong, C.-H. Lee, J. Yoo, Y.-J. Kim, J. Jeong, M. Kim, G.-C. Yi, Emission color-tuned light-emitting diode microarrays of nonpolar InxGa1–xN/GaN multishell nanotube heterostructures, Scientific Reports 5 (2015).
[15] M. Tchernycheva, P. Lavenus, H. Zhang, A.V. Babichev, G. Jacopin, M. Shahmohammadi, F.H. Julien, R. Ciechonski, G. Vescovi, O. Kryliouk, InGaN/GaN Core–Shell Single Nanowire Light Emitting Diodes with Graphene-Based P-Contact, Nano Letters 14 (2014) 2456-2465.

[16] M. Nami, I.E. Stricklin, K.M. DaVico, S. Mishkat-Ul-Masabih, A.K. Rishinaramangalam, S.R.J. Brueck, I. Brener, D.F. Feezell, Carrier Dynamics and Electro-Optical Characterization of High-Performance GaN/InGaN Core-Shell Nanowire Light-Emitting Diodes, Sci Rep 8 (2018) 501.

[17] F. Qian, Y. Li, S. Gradecak, H.G. Park, Y. Dong, Y. Ding, Z.L. Wang, C.M. Lieber, Multi-quantum-well nanowire heterostructures for wavelength-controlled lasers, Nat Mater 7 (2008) 701-706.

[18] Q. Li, G.T. Wang, Spatial distribution of defect luminescence in GaN nanowires, Nano Lett 10 (2010) 1554-1558.

[19] A. Uedono, T. Watanabe, S. Kimura, Y. Zhang, M. Lozac'h, L. Sang, S. Ishibashi, N. Oshima, R. Suzuki, M. Sumiya, Vacancy-type defects in InxGa1−xN grown on GaN templates probed using monoenergetic positron beams, Journal of Applied Physics 114 (2013) 184504.

[20] S.F. Chichibu, K. Hazu, Y. Ishikawa, M. Tashiro, H. Namita, S. Nagao, K. Fujito, A. Uedono, Time-resolved photoluminescence, positron annihilation, and Al0.23Ga0.77N/GaN heterostructure growth studies on low defect density polar and nonpolar freestanding GaN substrates grown by hydride vapor phase epitaxy, Journal of Applied Physics 111 (2012) 103518.

[21] D.J. Carter, M. Fuchs, C. Stampfl, Vacancies in GaN bulk and nanowires: effect of self-interaction corrections, J Phys Condens Matter 24 (2012) 255801.

[22] S. Chichibu, A. Uedono, K. Kojima, H. Ikeda, K. Fujito, S. Takashima, M. Edo, K. Ueno, S. Ishibashi, The origins and properties of intrinsic nonradiative recombination centers in wide bandgap GaN and AlGaN, Journal of Applied Physics 123 (2018) 161413.

[23] K. Shima, H. Iguchi, T. Narita, K. Kataoka, K. Kojima, A. Uedono, S.F. Chichibu, Room-temperature photoluminescence lifetime for the near-band-edge emission of (000 1 ¯) p-type GaN fabricated by sequential ion-implantation of Mg and H, Applied Physics Letters 113 (2018) 191901.

[24] C. Haller, J.-F. Carlin, G. Jacopin, W. Liu, D. Martin, R. Butté, N. Grandjean, GaN surface as the source of non-radiative defects in InGaN/GaN quantum wells, Applied Physics Letters 113 (2018) 111106.

[25] C. Haller, J.-F. Carlin, M. Mosca, M.D. Rossell, R. Erni, N. Grandjean, InAlN underlayer for near ultraviolet InGaN based light emitting diodes, Applied Physics Express 12 (2019) 034002.

[26] T. Obata, J.-i. Iwata, K. Shiraishi, A. Oshiyama, First principles studies on In-related nitride semiconductors, Journal of Crystal Growth 311 (2009) 2772-2775.

[27] K. Choi, M. Arita, Y. Arakawa, Selective-area growth of thin GaN nanowires by MOCVD, Journal of Crystal Growth 357 (2012) 58-61.

[28] W. Liu, C. Mounir, G. Rossbach, T. Schimpke, A. Avramescu, H.J. Lugauer, M. Strassburg, U. Schwarz, B. Deveaud, G. Jacopin, Spatially dependent carrier dynamics in single InGaN/GaN core-shell microrod by time-resolved cathodoluminescence, Applied Physics Letters 112 (2018) 052106.

[29] A.K. Rishinaramangalam, M. Nami, D.M. Shima, G. Balakrishnan, S.R.J. Brueck, D.F. Feezell, Reduction of reverse-leakage current in selective-area-grown GaN-based core-shell nanostructure LEDs using AlGaN layers, physica status solidi (a) 214 (2017) 1600776.

[30] W.-Y. Jung, C.-M. Kwak, J.-B. Seol, J.K. Park, C.-G. Park, Y.K. Jeong, Observation of Anisotropic Growth and Compositional Discontinuity in AlGaN Electron-Blocking Layers on GaN Microrods, Crystal Growth & Design 18 (2018) 1593-1597.

[31] S. Grzanka, G. Franssen, G. Targowski, K. Krowicki, T. Suski, R. Czernecki, P. Perlin, M. Leszczyński, Role of the electron blocking layer in the low-temperature collapse of electroluminescence in nitride light-emitting diodes, Applied Physics Letters 90 (2007) 103507.

[32] M. Albrecht, L. Lymperakis, J. Neugebauer, J.E. Northrup, L. Kirste, M. Leroux, I. Grzegory, S. Porowski, H.P. Strunk, Chemically orderedAlxGa1−xNalloys: Spontaneous formation of natural quantum wells, Physical Review B 71 (2005).

[33] K.H. Warnick, Y. Puzyrev, T. Roy, D.M. Fleetwood, R.D. Schrimpf, S.T. Pantelides, Room-temperature diffusive phenomena in semiconductors: The case of AlGaN, Physical Review B 84 (2011).

[34] T.A. Henry, A. Armstrong, A.A. Allerman, M.H. Crawford, The influence of Al composition on point defect incorporation in AlGaN, Applied Physics Letters 100 (2012) 043509.

[35] M.A. Khan, M. Shatalov, H. Maruska, H. Wang, E. Kuokstis, III–nitride UV devices, Japanese journal of applied physics 44 (2005) 7191.

[36] M.R. Laskar, T. Ganguli, A.A. Rahman, A.P. Shah, M.R. Gokhale, A. Bhattacharya, MOVPE growth and characterization of a -plane AlGaN over the entire composition range, physica status solidi (RRL) - Rapid Research Letters 4 (2010) 163-165.

[37] H. Angerer, D. Brunner, F. Freudenberg, O. Ambacher, M. Stutzmann, R. Höpler, T. Metzger, E. Born, G. Dollinger, A. Bergmaier, S. Karsch, H.J. Körner, Determination of the Al mole fraction and the band gap bowing of epitaxial AlxGa1−xN films, Applied Physics Letters 71 (1997) 1504-1506.

[38] F. Yun, M.A. Reshchikov, L. He, T. King, H. Morkoç, S.W. Novak, L. Wei, Energy band bowing parameter in AlxGa1−xN alloys, Journal of Applied Physics 92 (2002) 4837-4839.

[39] M. Brubaker, K. Genter, A. Roshko, P. Blanchard, B. Spann, T. Harvey, K. Bertness, UV LEDs based on pin core-shell AlGaN/GaN nanowire heterostructures grown by N-polar selective area epitaxy, Nanotechnology (2019).

[40] C.G. Van de Walle, C. Stampfl, J. Neugebauer, M. McCluskey, N. Johnson, Doping of Aigan Alloys, MRS Online Proceedings Library Archive 537 (1998).

[41] K.B. Nam, M.L. Nakarmi, J.Y. Lin, H.X. Jiang, Deep impurity transitions involving cation vacancies and complexes in AlGaN alloys, Applied Physics Letters 86 (2005) 222108.

[42] G.S. Huang, H.H. Yao, H.C. Kuo, S.C. Wang, Effect of growth conditions on the Al composition and quality of AlGaN film, Materials Science and Engineering: B 136 (2007) 29-32.

[43] V. Jindal, F. Shahedipour-Sandvik, Density functional theoretical study of surface structure and adatom kinetics for wurtzite AlN, Journal of Applied Physics 105 (2009) 084902.

[44] L. Lymperakis, J. Neugebauer, Large anisotropic adatom kinetics on nonpolar GaN surfaces: Consequences for surface morphologies and nanowire growth, Physical Review B 79 (2009).

[45] A.M. Munshi, D.-C. Kim, C.P. Heimdal, M. Heilmann, S.H. Christiansen, P.E. Vullum, A.T.J. van Helvoort, H. Weman, Selective area growth of AlGaN nanopyramid arrays on graphene by metal-organic vapor phase epitaxy, Applied Physics Letters 113 (2018) 263102.

[46] M. Sawicka, C. Chèze, H. Turski, J. Smalc-Koziorowska, M. Kryśko, S. Kret, T. Remmele, M. Albrecht, G. Cywiński, I. Grzegory, C. Skierbiszewski, Growth mechanisms in semipolar and nonpolar m-plane AlGaN/GaN structures grown by PAMBE under N-rich conditions, Journal of Crystal Growth 377 (2013) 184-191.

An impressive enhancement of cathodoluminescence was achieved in coaxial GaInN/GaN multiple-quantum-shells nanowires by employing an AlGaN undershell for trapping point defects.